SPANDIDOS
PUBLICATIONS

PD-L1 mediates triple-negative breast cancer evolution via the regulation of TAM/M2 polarization

ZIQI MENG[1,2], RUI ZHANG[1,2], XUWEI WU[1,2], MEIHUA ZHANG[3] and TIEFENG JIN[1,2]

[1]Department of Pathology and Cancer Research Center, [2]Key Laboratory of the Science and Technology Department of Jilin Province, and [3]Health Examination Centre, Yanbian University Hospital, Yanji, Jilin 133002, P.R. China

Abstract. Tumor-associated macrophages/M2-type (TAM/M2) play a key role in the metastasis and angiogenesis of cancer, and are considered to be critical targets for cancer treatment. However, it remains unclear whether α-programmed death-ligand 1 (αPD-L1; PD-L1 inhibitor) inhibits tumor progression via targeting TAMs. In the present study, it was demonstrated that αPD-L1 significantly inhibited IL-13-induced TAM/M2 polarization *in vitro*. Moreover, αPD-L1 inhibited the epithelial-mesenchymal transition (EMT) process and the stemness of triple-negative breast cancer (TNBC) cells, which were mediated via the reversal of TAM/M2 polarization. This therefore inhibited the migration and angiogenesis of TNBC cells. Furthermore, αPD-L1 prevented STAT3 phosphorylation and nuclear translocation, which resulted in the arrest of TAM/M2 polarization. *In vivo* experiments further demonstrated that αPD-L1 reduced the number of lung metastases without affecting tumor growth. Moreover, αPD-L1 reduced the expression levels of TAM/M2, EMT, stemness and vascular markers in tumor tissues. In summary, these data suggest that αPD-L1 plays a vital role in the anti-metastasis and anti-angiogenesis of TNBC *in vitro* and *in vivo* via the inhibition of TAM/M2 polarization. These findings may thus provide a novel therapeutic strategy for clinically refractory TNBC.

Correspondence to: Professor Tiefeng Jin, Department of Pathology and Cancer Research Center, Yanbian University Hospital, 977 Gong Yuan Road, Yanji, Jilin 133002, P.R. China
E-mail: jintf@ybu.edu.cn

Dr Meihua Zhang, Health Examination Centre, Yanbian University Hospital, 977 Gong Yuan Road, Yanji, Jilin 133002, P.R. China
E-mail: zhangmeihua81@hotmail.com

Introduction

Breast cancer is the most common type of cancer and the main cause of cancer-related mortality among women (1). It has previously been reported that breast cancer accounts for ~11.7% of all global cancer cases and 15.5% of all female cancer-related deaths (2). Breast cancer is divided into the following four subtypes according to its molecular phenotypes: i) Luminal A; ii) Luminal B; iii) human epidermal growth factor receptor-2; and iv) triple-negative breast cancer (TNBC) (3). TNBC accounts for ~15% of all breast cancer cases (4) and is characterized by an obvious heterogeneity, an early age of onset, a high risk of visceral metastasis, high tumor invasiveness and a high histological grade (5). Due to the high tumor heterogeneity of TNBC and the lack of a clear therapeutic target, effective treatments are still lacking.

The tumor microenvironment (TME) plays a key role in the occurrence and development of cancers (6). Tumor cells promote the evolution of cancer by altering the TME to create favorable conditions for their own survival (7). Tumor-associated macrophages (TAMs) are the main immune cells in the TME and account for 50-80% of mesenchymal cells (8). TAMs have a strong plasticity and polarize into different phenotypes under the stimulation of the TME and cytokines. Moreover, TAMs can be divided into macrophages activated by the classical pathway, TAM/M1, or the alternative pathway, TAM/M2, according to their different polarization modes. TAM/M1 mainly contributes towards tumor inhibition, whereas TAM/M2 has more tumor promoting properties (9). Moreover, ~90% of breast cancer-related deaths are caused by metastasis (10). Furthermore, cytokines in the TME interact with tumor cells and thereby play a crucial role in the process of tumor metastasis (11). TAM/M2 are associated with a poor prognosis of breast, colorectal and gastric cancer (12-14). Furthermore, epithelial-mesenchymal transition (EMT) is associated with tumor metastasis and a poor prognosis (15). A previous study reported that TAMs enhanced the metastasis of colorectal cancer cells by inducing the EMT process (16). Cancer stem cells (CSCs) are self-regenerative and have a high carcinogenic potential; they are thus considered to be related to chemotherapeutic resistance, metastasis and recurrence (17). TAM-derived cytokines enhance the stemness of cancer via the EMT process (18). TAM/M2 induce angiogenesis and secrete pro-angiogenic factors, such as vascular endothelial growth

factor (VEGF), degrade the tumor extracellular matrix and help tumor cells to evade the immune system. These factors help promote tumor metastasis, immunosuppression and drug resistance, and provide nutrition and metastasis pathways that contributes towards tumor growth (19). Therefore, reversing the polarization of TAM/M2, reducing their recruitment and blocking the tumor-promoting function of TAM/M2 may prove to be a potential novel antitumor therapeutic strategy.

Programmed death receptor-1 (PD-1) is an inhibitory co-receptor that binds to programmed death ligand-1 (PD-L1) to effectively inhibit T-cell activity, thereby reducing the T-cell recognition of tumor cells and enabling tumor cells to evade immune supervision (20). The expression of PD-1 and PD-L1 in patients with TNBC are higher compared with other molecular types of breast cancer (21). PD-L1 inhibitors have a long-lasting effect on advanced TNBC (22). A previous study reported that tumor drug resistance significantly restricted the later efficacy of PD-1/PD-L1 inhibitors (23). PD-L1 expression in the TME of tumor cells and host immune cells assists tumor cell immune evasion. Therefore, monitoring PD-L1 expression levels in tumor tissues is more important than monitoring PD-L1 expression levels in tumor cells (24). The expression of PD-L1 plays a decisive role in host immune cells, rather than tumor cells (25). Therefore, the expression of PD-L1 in TAMs plays a key role in tumor progression. It can thus be hypothesized that TNBC may induce TAM/M2 polarization and promote tumor evolution. However, whether αPD-L1 inhibits TNBC malignant progression by reversing TAM/M2 polarization has not yet been reported, at least to the best of our knowledge. Therefore, the present study aimed to investigate the role of αPD-L1 in the regulation of TAM polarization in the TME of TNBC, to reveal the molecular role of αPD-L1 in reversing TAM polarization towards the M2 phenotype, and to provide a novel therapeutic strategy for refractory TNBC.

Materials and methods

Cells and cell culture. The Yanbian University Cancer Research Center (Yanji, China) supplied the human TNBC (MDA-MB-231 and Hs578T) cell lines, the mouse 4T1 cell line, immortalized HUVECs, the human monocyte THP-1 cell line, and the mouse macrophage RAW264.7 cell line. All cell lines were cultured in RPMI-DMEM (Gibco; Thermo Fisher Scientific, Inc.) containing 10% FBS (Gibco; Thermo Fisher Scientific, Inc.) and 1% streptomycin-penicillin (100 U/ml). THP-1 cells were differentiated into macrophages using 100 ng/ml phorbol-12-myristate 13-acetate (PMA; Sigma-Aldrich; Merck KGaA) for 24 h. The cells were cultured at 37°C in an atmosphere of 5% CO_2.

Flow cytometry. The RAW264.7 cells ($5x10^5$) were washed twice with cell staining buffer (Biolegend, Inc.) and were subsequently fixed using fixation buffer (Biolegend, Inc.). The cell membranes were broken using permeabilization buffer (Biolegend, Inc.). The cells were then stained with CD68-FITC (1:100; cat. no. 137006; Biolegend, Inc.), CD206-phycoerythrin (1:100; cat. no. 141706; Biolegend, Inc.) and CD86-allophycocyanin (1:100; cat. no. 105011; Biolegend, Inc.) antibodies at 4°C for 2 h (1:100; Biolegend, Inc.). The cells were subsequently suspended in 500 μl cell staining buffer and examined using a BD Accuri C6 flow cytometer (BD Biosciences). FlowJo V10.5.3 (TreeStar, Inc.) software was employed for analysis.

Western blot analysis. The MDA-MB-231, Hs578T, RAW264.7 and THP-1 cells were collected and the total protein was extracted using RIPA lysate (RIPA lysis buffer: PMSF, 100:1). Nuclear and cytoplasmic proteins was isolated using a Nuclear and Cytoplasmic Protein Extraction kit (Beyotime Institute of Biotechnology) according to the manufacturer's instructions. The protein concentration was determined and quantified using a BCA kit (Roche Diagnostics). Proteins (30 μg per lane) were separated using SDS-PAGE (8 and 10%) and the separated proteins were then transferred a to PVDF membrane (MilliporeSigma). The membrane was placed in 5% non-fat milk (BD Biosciences) and blocked for 2 h at room temperature to remove non-specific binding sites. The membranes were incubated with the primary antibodies at 4°C overnight and subsequently with the secondary antibodies at room temperature for 1 h. Primary antibodies specific for the following proteins were used: PD-L1 (1:1,000; cat. no. 60475 and 85164; CST Biological Reagents Co., Ltd.), CD86 (1:1,000; cat. no. sc-28347; Santa Cruz Biotechnology, Inc.), CD206 (1:1,000; cat. no. 24595; CST Biological Reagents Co., Ltd.), VEGF (1:1,000; cat. no. sc-7269; Santa Cruz Biotechnology, Inc.), MMP2 (1:1,000; cat. no. sc-13594; Santa Cruz Biotechnology, Inc.), MMP9 (1:1,000; cat. no. sc-393859; Santa Cruz Biotechnology, Inc.), E-cadherin (1:1,000; cat. no. 14472; CST Biological Reagents Co., Ltd.), zonula occludens-1 (ZO-1; 1:1,000; cat. no. 8193; CST Biological Reagents Co., Ltd.), N-cadherin (1:1,000; cat. no. sc-8424; Santa Cruz Biotechnology, Inc.), vimentin (1:1,000; cat. no. sc-6260; Santa Cruz Biotechnology, Inc.), Slug (1:1,000; cat. no. sc-166476; Santa Cruz Biotechnology, Inc.), Twist (1:1,000; cat. no. sc-81417; Santa Cruz Biotechnology, Inc.), CD44 (1:1,000; cat. no. 3570; CST Biological Reagents Co., Ltd.), octamer-binding transcription factor 4 (Oct4; 1:1,000; cat. no. 75643; CST Biological Reagents Co., Ltd.), Nanog (1:1,000; cat. no. sc-374103; Santa Cruz Biotechnology, Inc.), Bmi1 (1:1,000; cat. no. sc-390443; Santa Cruz Biotechnology, Inc.), Sox2 (1:1,000; cat. no. sc-365823; Santa Cruz Biotechnology, Inc.), CCAAT/enhancer-binding protein β (CEBPβ; 1:1,000; cat. no. sc-7962; Santa Cruz Biotechnology, Inc.), phosphorylated (p-)ERK (1:1,000; cat. no. 4695; CST Biological Reagents Co., Ltd.), ERK (1:1,000; cat. no. 48303; CST Biological Reagents Co., Ltd.), p-STAT6 (1:1,000; cat. no. 56554; CST Biological Reagents Co., Ltd.), STAT6 (1:1,000; cat. no. sc-374021; Santa Cruz Biotechnology, Inc.), p-STAT3 (1:1,000; cat. no. 9145; CST Biological Reagents Co., Ltd.), STAT3 (1:1,000; cat. no. 9139; CST Biological Reagents Co., Ltd.), β-actin (1:1,000; cat. no. CW0096; CWBio Technology Co., Ltd.), GAPDH (1:1,000; cat. no. CW0100M; CWBio Technology Co., Ltd.) and H3 (1:1,000; cat. no. 60932; CST Biological Reagents Co., Ltd.). Three different loading controls were used (β-actin, GAPDH and H3) in this experiment. Horseradish peroxidase-conjugated secondary antibodies, including goat anti-mouse (1:3,000; cat. no. ZB-2305; ZSGB-BIO Technology Co., Ltd.) and goat anti-rabbit (1:3,000; cat. no. ZB-2301; ZSGB-BIO Technology Co., Ltd.) antibodies were used. Enhanced chemiluminescence kit (CWBio Technology Co., Ltd.) was used to detect antibody signals and images were collected. ImageJ (v. 1.48; National Institutes of Health) software was employed for analysis.

Immunofluorescence (IF) staining. MDA-MB-231, Hs578T and RAW264.7 cells, with a 30% fusion rate, were seeded into six-well plates, fixed with anhydrous methanol at room temperature for 15 min and permeated with 0.5% Triton X-100 (CWBio Technology Co., Ltd.) at room temperature for 10 min. The cells were then blocked with 3% BSA (Beijing Solarbio Science & Technology) at room temperature for 2 h. Subsequently, the cells were incubated with primary antibody in 3% BSA at 4°C overnight. Primary antibodies specific for the following proteins were used: CD206 (1:100; cat. no. 24595; CST Biological Reagents Co., Ltd.), E-cadherin (1:100; cat. no. 14472; CST Biological Reagents Co., Ltd.), Vimentin (1:100; cat. no. sc-6260; Santa Cruz Biotechnology, Inc.), CD44 (1:100; cat. no. 3570; CST Biological Reagents Co., Ltd.), p-STAT3 (1:100; cat. no. 9145; CST Biological Reagents Co., Ltd.) and STAT3 (1:100; cat. no. sc-8059; Santa Cruz Biotechnology, Inc.). Following incubation with the primary antibodies, the cells were then incubated with Alexa Fluor 488 goat anti-rabbit IgG (1:400; cat. no. A11008; Invitrogen; Thermo Fisher Scientific, Inc.) or Alexa Fluor 568 goat anti-mouse IgG (1:400; cat. no. A11004; Invitrogen; Thermo Fisher Scientific, Inc.) at room temperature for 1 h. The cells were counterstained with DAPI and imaged using a Leica SP5II confocal microscope (Leica Microsystems GmbH).

ELISA. ELISA was performed according to the manufacturer's instructions. The concentrations of interleukin (IL)-10 (Mlbio; cat. no. ml037873; Shanghai Enzyme-linked Biotechnology Co., Ltd.) and IL-12 (Mlbio; cat. no. ml037868; Shanghai Enzyme-linked Biotechnology Co., Ltd.) in the RAW264.7 cell culture supernatants were determined using the corresponding kits.

MTT assay. The MDA-MB-231, Hs578T and RAW264.7 cells ($5x10^3$)/well were seeded and incubated in 96-well plates at 37°C for 24 h. Conditioned medium (CM) or drugs (IL-13, 30 ng/ml; and/or αPD-L1, 15 μg/ml) were added and the cells were further incubated at 37°C for 0, 24, 48 and 72 h. Subsequently, 100 μl MTT reagent (1 mg/ml; Beyotime Institute of Biotechnology) were added to each well and the cells were incubated at 37°C for 4 h under the same conditions. Subsequently, 100 μl DMSO (Beijing Solarbio Science & Technology) were added to each well and the optical density at 490 nm was assessed using a full-wavelength multifunctional microplate reader (Tecan, Inc.). At least five wells/group were analyzed and the experiment was repeated three times.

Apoptosis assay. The MDA-MB-231, Hs578T and RAW264.7 cells ($1x10^6$) were washed twice with binding buffer and were then stained using the Annexin V-FITC Apoptosis Detection kit (BD Biosciences) according to the manufacturer's instructions. The cells were analyzed using a BD Accuri C6 flow cytometer (BD Biosciences). FlowJo V10.5.3 (TreeStar, Inc.) software was employed for analysis.

Cell morphology. RAW264.7 cells, with a 30% fusion rate, were incubated in 6-well plates at 37°C for 12 h and were then treated with the TAM/M2-inducing factor, IL-13 (10, 20 and 30 ng/ml; Biolegend, Inc.) and/or αPD-L1

(15 μg/ml; 10F.9G2 monoclonal antibody; cat no. BE0101; Bio X Cell) at 37°C for 48 h. Morphological cell changes were observed using a microscope and images were obtained (IX73, Olympus Corporation).

CM preparation. RAW264.7 and THP-1 (PMA) cells were treated with IL-13 and/or αPD-L1 at 37°C for 48 h. The cells were then cultured in serum-free medium at 37°C for 24 h, and three types of CM (control, IL-13 and IL-13 + αPD-L1) were prepared. The CM was directly used in the assays or stored at -80°C. The CM was filtered and 2% FBS was added.

Transwell assay. The MDA-MB-231 and Hs578T cells ($5x10^4$) in 100 μl serum-free RPMI-DMEM were seeded into the upper chamber. The bottom chamber was filled with RPMI-DMEM with 10% FBS. The cells were incubated at 37°C for 6 h. The upper chambers were replaced with different types of CM. Cells passing through the subsurface of the filtration membrane were fixed with 4% paraformaldehyde at room temperature for 20 min and were then stained with 0.1% crystal violet at room temperature for 20 min. In total, three fields (magnification, x200) were randomly selected for imaging using a microscope (IX73; Olympus Corporation). Image-J software (v. 1.46; National Institutes of Health) was used to quantify the number of cells in each field.

Wound healing assay. Cells, with a 80% fusion rate, were incubated in six-well plates at 37°C for 24 h. The wound was scratched vertically using a 200 μl pipette tip and the plates were washed three times with PBS to remove dead cells in the well. The cells with serum-free CM (containing IL-13 and/or αPD-L1) were imaged using a microscope (IX73; Olympus Corporation) at 0, 12 and 24 h.

Soft-agar colony-forming assay. In 96-well plates 1% agarose (Beijing Solarbio Science & Technology) in complete medium was applied and was solidified at 37°C for 30 min. The MDA-MB-231 and Hs578T cells ($1x10^3$) were mixed with 0.3% agarose in CM and were plated on top of the bottom layer of 1% agarose. Subsequently, complete medium was applied on top of the cell layer. The number and size of the colonies were observed using a microscope (citation 5; BioTek Instruments, Inc.) after 14 days.

Endothelial tube formation assay. Matrigel (BD Biosciences) and RPMI-DMEM were diluted 1:1 in 96-well plates and solidified at 37°C for 4 h. HUVECs ($2x10^4$) were incubated in 2:1 diluted CM and culture medium (Gibco; Thermo Fisher Scientific, Inc.) containing 10% FBS (Gibco; Thermo Fisher Scientific, Inc.) and 1% streptomycin-penicillin (100 U/ml) at 37°C for 4 h. The capillary structure was imaged using a microscope (IX73; Olympus Corporation).

Cell co-culture system. RAW264.7 cells ($5x10^4$) were added to 600 μl RPMI-DMEM with 10% FBS, which was added to the bottom chamber. The MDA-MB-231 or Hs578T cells ($1x10^5$) were added to 100 μl RPMI-DMEM with 10% FBS, which was added to the upper chamber. The cells were co-cultured at 37°C for 6 h and subsequently αPD-L1 (15 μg/ml) was added at 37°C for 48 h. The supernatant was harvested for use

in ELISA, and the RAW264.7 cells were harvested for use in western blot analysis and flow cytometry.

The RAW264.7 cells ($5x10^4$) in 100 μl RPMI-DMEM with 10% FBS were seeded into the upper chamber. The MDA-MB-231 or Hs578T cells ($1x10^5$) in 100 μl RPMI-DMEM with 10% FBS were seeded into the bottom chamber. The cells were co-cultured at 37˚C for 6 h and αPD-L1 subsequently incubated at 37˚C for 48 h. The MDA-MB-231 or Hs578T cells were then collected for use in western blot analysis, wound healing and Transwell assays.

The following six groups were established: i) Negative control group, RAW264.7 cells were cultured separately; ii) positive control group, RAW264.7 cells were treated with IL-13 to produce TAM/M2; iii) co-culture group 1, RAW264.7 cells were co-cultured with MDA-MB-231 cells; iv) co-culture treated group 1, RAW264.7 cells were co-cultured with MDA-MB-231 cells with αPD-L1 treatment; v) co-culture group 2, RAW264.7 cells were co-cultured with Hs578T cells; vi) co-culture treated group 2, RAW264.7 cells were co-cultured with Hs578T cells with αPD-L1 treatment.

Animal experiments. The animal experiments were conducted between November, 2021 to December, 2021. A total of 20 female BALB/c mice (age, 5 weeks, weighing ~20 g) were purchased from Beijing Vital River Laboratory Animal Technology Co., Ltd. All mice were housed under specific-pathogen-free conditions (temperature, 22˚C; humidity, 50%; light/dark cycle, 12/12 h), the animals were also provided with free access to food and water, and the padding was replaced twice a week. Animal health and behavior were monitored every day. The 4T1 cells ($5x10^5$/100 μl) were subcutaneously injected into the right flanks of the mice to establish a tumor model. After the tumors were palpable, the mice were randomly divided into the negative control (n=5) and αPD-L1 group (n=5). αPD-L1 (200 μg) was administered intraperitoneally to the mice once a day every 3 days (26). Tumor size was measured every 3 days and tumor volume was calculated using the following formula: Length x width^2 x0.5. The animals were sacrificed 25 days after the αPD-L1 treatment. For detecting lung metastases, 4T1 cells ($1x10^5$/100 μl) were injected into the tail vein of the mice. After 7 days, the mice were randomly divided into the negative control (n=5) and αPD-L1 group (n=5). αPD-L1 (200 μg) was administered intraperitoneally to the mice once a day every 3 days. The animals were sacrificed at 45 days after the αPD-L1 treatment. The humane endpoints of the experiment were as follows: i) Tumor burden, ≥10% body weight; ii) tumor volume, >2,000 mm^3; iii) weight loss, ≥20% body weight; iv) ulceration or infection on tumor; v) no movement for >24 h; and vi) no eating or drinking. In this experiment, no mice were found dead. All mice were sacrificed by cervical dislocation following an intraperitoneal injection of sodium pentobarbital (30 mg/kg) and sacrifice was confirmed when the mice had stopped breathing and did not respond to stimulation. The lungs were collected and the surface nodules were quantified. The tumor and lung tissues were fixed with 10% formalin at 4˚C for 24 h. The paraffin-embedded tumor tissues were sliced into 4-μm-thick sections. The expression of the markers was confirmed using immunohistochemical staining. Animal euthanasia was performed via cervical dislocation under 2%

isoflurane anesthesia. The present study was approved by the Animal Ethics Committee of Yanbian University (approval no. YD20220916004), and was performed according to the guidelines of the Committee on Animal Research and Ethics.

Hematoxylin and eosin (H&E). Tumor and lung tissue sections were dewaxed and rehydrated, stained with H&E (ZSGB-BIO Technology Co., Ltd.) at room temperature for 5 min and the stained tissue was evaluated under a microscope (IX73; Olympus Corporation).

Immunohistochemistry (IHC). Tumor and lung tissue sections were dewaxed and dehydrated. Subsequently, antigen retrieval was performed using microwave heating in 10 mM citrate buffer (pH 7.0) at 80˚C for 20 min. Endogenous peroxidase was blocked with 3% H_2O_2 (ZSGB-BIO Technology Co., Ltd.) at room temperature for 30 min. The tissue sections were incubated with primary antibodies at 4˚C overnight. Primary antibodies specific for the following proteins were used: CD206 (1:100; cat. no. 24595; CST Biological Reagents Co., Ltd.), E-cadherin (1:100; cat. no. 14472; CST Biological Reagents Co., Ltd.), vimentin (1:100; cat. no. sc-6260; Santa Cruz Biotechnology, Inc.), CD44 (1:100; cat. no. 3570; CST Biological Reagents Co., Ltd.), VEGF (1:100; cat. no. sc-7269; Santa Cruz Biotechnology, Inc.). Following incubation with the primary antibodies, the samples were incubated with horseradish peroxidase-conjugated secondary antibody (cat. no. PV9005; ZSGB-BIO Technology Co., Ltd.) at room temperature for 1 h. The samples were stained using DAB (ZSGB-BIO Technology Co., Ltd.) at room temperature for 5 min and counterstained with hematoxylin at room temperature for 1 min. The images were obtained using a microscope (IX73; Olympus Corporation).

Statistical analysis. GraphPad Prism 8.0 software (GraphPad Software, Inc.) was used for statistical analysis. A two-tailed unpaired Student's t-test was used to compare the mean values of two groups. One-way ANOVA with Tukey's post hoc test were used to compare the mean values of multiple groups. All experiments were repeated in triplicate and their mean values are presented as the mean ± SD. $P<0.05$ was considered to indicate a statistically significant difference.

Results

αPD-L1 reverses TAM/M2 polarization. RAW264.7 cells were treated with continuous concentrations of the TAM/M2-inducing factor, IL-13 (0, 10, 20 and 30 ng/ml) for 48 h. IF staining, western blot analysis and ELISA demonstrated that IL-13 promoted the levels of the TAM/M2 marker, CD206, in the RAW264.7 cell cytoplasm and the secretion of IL-10 in a concentration-dependent manner. IL-13 at 30 ng/ml had the most pronounced effect and this concentration was selected for use in further experiments (Fig. 1A-D). The RAW264.7 cells were treated with continuous concentrations of αPD-L1 for 24, 48 and 72 h. The results of MTT assay demonstrated that αPD-L1 at concentrations ≤15 μg/ml did not affect the proliferation of the RAW264.7 cells. αPD-L1 at a concentration of 15 μg/ml was thus selected for use in further experiments (Fig. 1E).
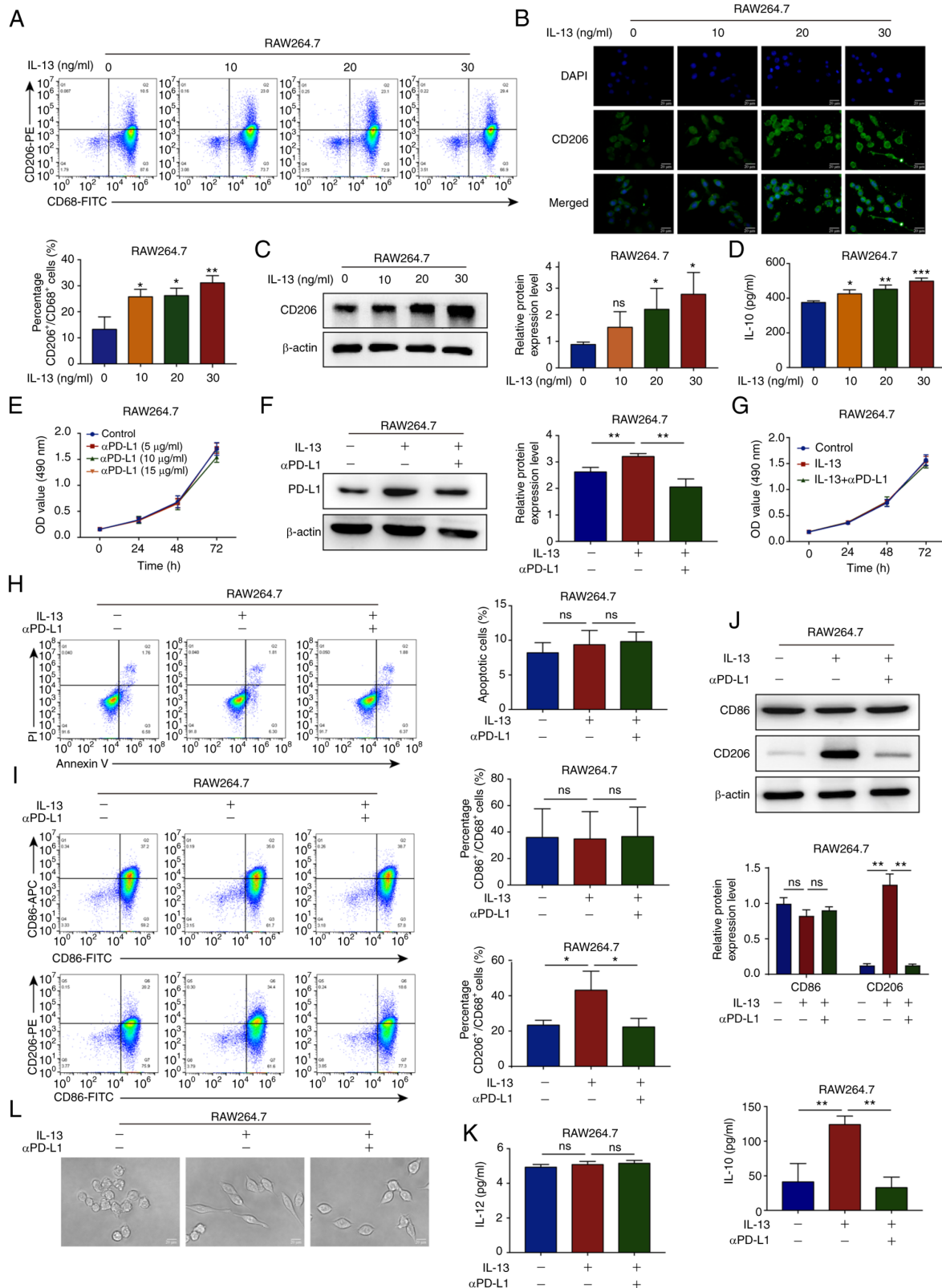
Figure 1. αPD-L1 reverses TAM/M2 polarization. (A) Flow cytometry was used to determine the percentage of CD206+/CD68+ RAW264.7 cells (Q2 region) treated with IL-13 (0, 10, 20 and 30 ng/ml). (B and C) Immunofluorescence staining and western blot analysis were performed to determine the protein expression levels of CD206 in RAW264.7 cells treated with IL-13 (magnification, x400). The markers were all expressed in the cytoplasm. (D) ELISA was performed to determine the IL-10 levels in RAW264.7 cells treated with IL-13. (E) RAW264.7 cell viability was determined using MTT assay when the cells were treated with αPD-L1 (0, 5, 10 and 15 µg/ml). (F) Western blot analysis was used to determine the protein expression levels of PD-L1 in RAW264.7 cells treated with IL-13 (30 ng/ml) and/or αPD-L1 (15 µg/ml). (G) RAW264.7 cell proliferation was analyzed using MTT assay when the cells were treated with IL-13 and/or αPD-L1. (H) RAW264.7 cell apoptosis was analyzed using flow cytometry when the cells were treated with IL-13 and/or αPD-L1. (I and J) CD86 and CD206 expression levels in the RAW264.7 cells treated with IL-13 and/or αPD-L1 were determined using flow cytometry and western blot analysis. (K) IL-12 and IL-10 levels in RAW264.7 cells treated with IL-13 and/or αPD-L1 were assessed using ELISA. (L) RAW264.7 cell morphology was imaged using a microscope when the cells were treated with IL-13 and/or αPD-L1. $^*P<0.05$, $^{**}P<0.01$ and $^{***}P<0.001$, vs. control. ns, not significant; αPD-L1, programmed death-ligand 1 inhibitor; TAM/M2, tumor-associated macrophages/M2-type.

To examine the potential effects of macrophages on TNBC progression, 100 ng/ml PMA were used to induce the differentiation of THP-1 cells into macrophages, which were characterized by the expression of the recognized macrophage marker, CD68 (Fig. S1A). To investigate the functions of αPD-L1 in TAM/M2 cells, the protein expression levels of PD-L1 were examined in TAM/M2 cells using western blot analysis. The results demonstrated that the PD-L1 protein expression levels were upregulated in the TAM/M2 cells and that αPD-L1 downregulated the expression of PD-L1 (Figs. 1F and S1B). Subsequently, it was demonstrated that IL-13 (30 ng/ml) and/or αPD-L1 (15 μg/ml) had no notable effect on the proliferation and apoptosis of RAW264.7 cells, as shown by MTT and flow cytometric assays (Fig. 1G and H). The results of flow cytometry, western blot analysis and ELISA demonstrated that αPD-L1 inhibited the TAM/M2 marker, CD206, and the IL-10 levels induced by IL-13. However, the expression of the TAM/M1 marker, CD86, and the IL-12 levels were not markedly affected by IL-13 and/or αPD-L1 (Figs. 1I-K and S1B). To further investigate the effects of αPD-L1 on TAM/M2 polarization, changes in cell morphology were observed using a microscope. IL-13 stimulated the RAW264.7 cells and changed the morphology from a round or oval shape to a long spindle shape, whereas αPD-L1 inhibited cell extension (Fig. 1L). These data thus suggested that αPD-L1 inhibited TAM/M2 polarization.

αPD-L1 inhibits the TAM/M2-induced migration and angiogenesis of TNBC cells. The RAW264.7 and THP-1 cells were treated with IL-13 and/or αPD-L1 for 48 h and supernatant was replaced with serum-free medium for 24 h and then collected as CM (Fig. 2A). To examine the effects of αPD-L1 on the interaction between TAM/M2 and TNBC cells, it was determined that CM had no notable effect on the proliferation and apoptosis of TNBC cells, as shown by MTT assay and flow cytometry (Fig. 2B and C). Subsequently, wound healing and Transwell assays confirmed that the MDA-MB-231 and Hs578T cells treated with the CM of IL-13/RAW264.7 or IL-13/THP-1 cells exhibited an increased cell migration, whereas the CM of IL-13 + αPD-L1/RAW264.7 or IL-13 + αPD-L1/THP-1 cells reversed this phenomenon (Figs. 2D and E, and S1C and D).

Neovascularization in tumor tissues is an important condition for malignant tumor metastasis that is regulated via various chemokines in the TME (27). In the present study, to investigate the effects of αPD-L1 on angiogenesis via TAM/M2 polarization *in vitro*, an endothelial tube formation assay was performed. The results demonstrated that HUVECs treated with the CM of IL-13/RAW264.7 cells exhibited increased microtubule formation, whereas the CM of IL-13 + αPD-L1/RAW264.7 cells reversed this phenomenon (Fig. 2F). Subsequently, western blot analysis was performed and the results demonstrated that the MDA-MB-231 and Hs578T cells treated with the CM of IL-13/RAW264.7 or IL-13/THP-1 cells exhibited upregulated protein expression levels of VEGF, MMP2 and MMP9. However, the CM of IL-13 + αPD-L1/RAW264.7 or IL-13 + αPD-L1/THP-1 cells reversed this phenomenon (Figs. 2G and S1E). These data thus suggested that αPD-L1 inhibited TNBC cell migration and angiogenesis that was induced by TAM/M2 polarization.

αPD-L1 inhibits the TAM/M2-induced EMT process and the stemness of TNBC cells. To investigate whether αPD-L1 inhibits the EMT process of TNBC cells via the regulation of TAM polarization, western blot analysis and IF staining were performed. The results demonstrated that the MDA-MB-231 and Hs578T cells treated with the CM of IL-13/RAW264.7 or IL-13/THP-1 cells exhibited upregulated protein expression levels of the mesenchymal markers, N-cadherin, vimentin, Slug and Twist. Furthermore, the protein expression levels of the epithelial markers, E-cadherin and ZO-1 were down-regulated. However, the MDA-MB-231 and Hs578T cells treated with the CM of IL-13 + αPD-L1/RAW264.7 or IL-13 + αPD-L1/THP-1 cells exhibited a reversal of this phenomenon (Figs. 3A and B, and S1E).

Tumor cells express high levels of stem cell surface markers following EMT progression, which indicates that these cells have become stem cells (28). In the present study, to investigate whether αPD-L1 inhibits the stemness of TNBC cells via the regulation of TAM/M2 polarization, western blot analysis and IF staining were performed. The results demonstrated that the MDA-MB-231 and Hs578T cells treated with the CM of IL-13/RAW264.7 or IL-13/THP-1 cells exhibited upregulated protein expression levels of the stemness markers, CD44, Oct4, Nanog, Bmi1 and Sox2. However, the MDA-MB-231 and Hs578T cells treated with the CM of IL-13 + αPD-L1/RAW264.7 or IL-13 + αPD-L1/THP-1 exhibited a reversal of this phenomenon (Figs. 3C and D, and S1F). The present study then investigated whether αPD-L1 inhibits CSC properties without affecting cell proliferation. There is increasing evidence to suggest that 3D cell culture is a more accurate reflection of the TME 2D culture (29). Therefore, the soft agar colony formation assay, a technique widely used to assess CSC proliferation, was used herein (30). The results demonstrated that TNBC cells treated with the CM of IL-13/RAW264.7 cells exhibited an increased colony number and size, whereas the CM of IL-13 + αPD-L1/RAW264.7 reversed this phenomenon (Fig. S2). These data thus suggested that αPD-L1 inhibited the EMT process and the stemness of TNBC cells by reversing TAM/M2 polarization, which thereby inhibited TNBC metastasis and angiogenesis.

αPD-L1 reverses TAM/M2 polarization in the co-culture system. The effects of TAM/M2 polarization on TNBC cells were identified and therefore a co-culture system of TAMs and TNBC cells was established to simulate this interaction in the TME (Fig. 4A). Flow cytometry and western blot analysis confirmed that the percentage of CD206+/CD68+ (TAM/M2) cells and the levels of CD86 and CD206 in the RAW264.7 cells co-cultured with TNBC cells were upregulated, whereas αPD-L1 downregulated the percentage of CD206+/CD68+ cells. However, the percentages of CD86+/CD68+ (TAM/M1) cells were not significantly altered in the co-culture system with or without αPD-L1 (Fig. 4B and C). To further support these results, ELISA was performed and the results demonstrated that the IL-10 levels in the positive control group, co-culture group 1 and co-culture group 2 were increased, whereas αPD-L1 reversed this phenomenon. However, the IL-12 levels were not altered by the co-culture system with or without αPD-L1 (Fig. 4D). These data suggested that αPD-L1 regulated the interaction between TAMs and TNBC cells.
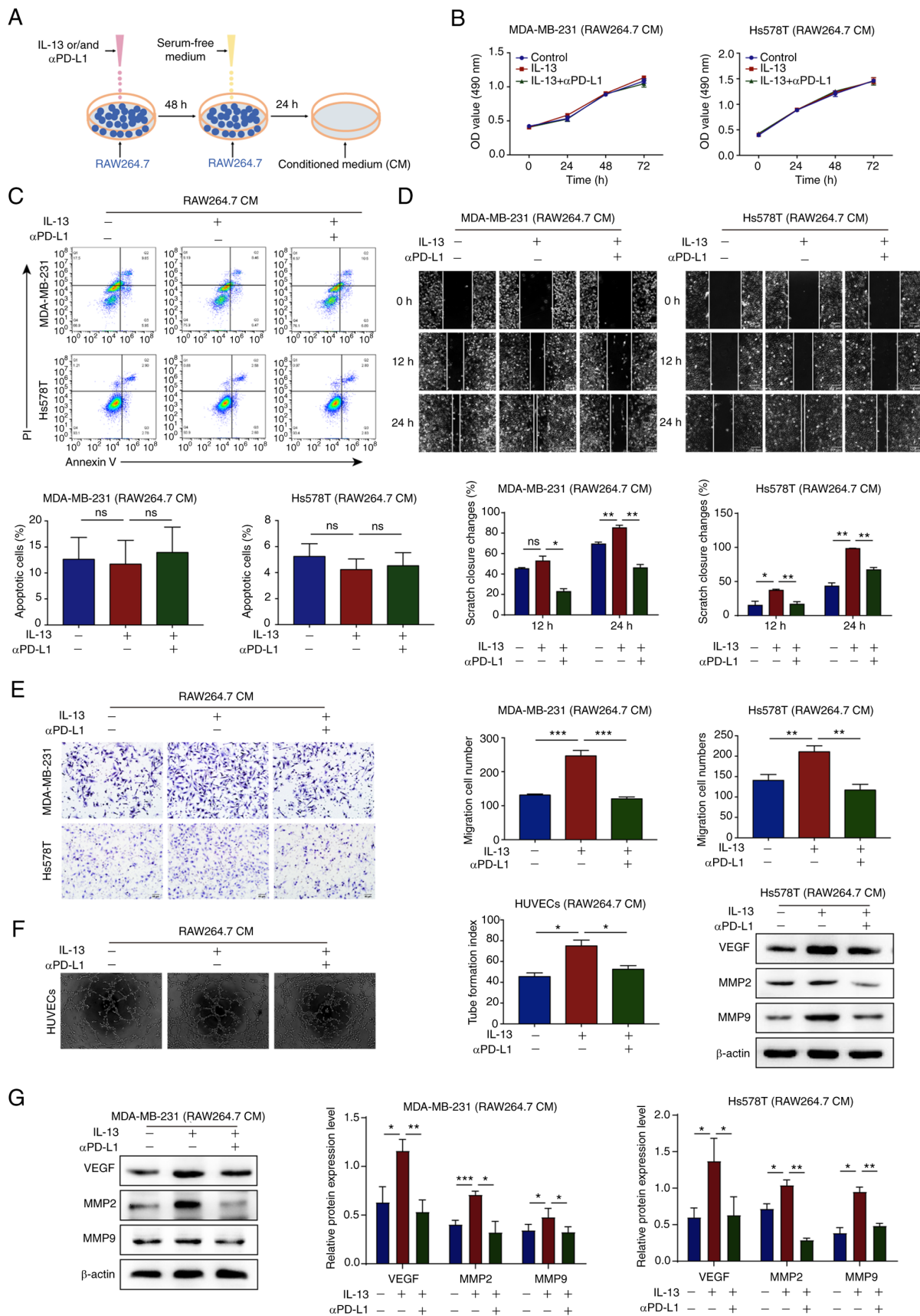
Figure 2. αPD-L1 inhibits the migration and angiogenesis of TNBC promoted by TAM/M2. (A) Schematic diagram of the RAW264.7 cell CM preparation. (B and C) MDA-MB-231 and Hs578T cell proliferation and apoptosis were examined using MTT assay and flow cytometry when the cells were treated with CM. (D and E) MDA-MB-231 and Hs578T cell migration was assessed using wound healing and Transwell assays when the cells were treated with CM (magnification, x200). (F) HUVEC microtubule formation capacity was assessed using the endothelial tube formation assay when the cells were treated with CM. (G) VEGF, MMP2 and MMP9 protein expression levels in MDA-MB-231 and Hs578T cells treated with CM were examined using western blot analysis. *P<0.05, **P<0.01 and ***P<0.001. ns, not significant; αPD-L1, programmed death-ligand 1 inhibitor; TAM/M2, tumor-associated macrophages/M2-type; CM, conditional media; VEGF, vascular endothelial growth factor.
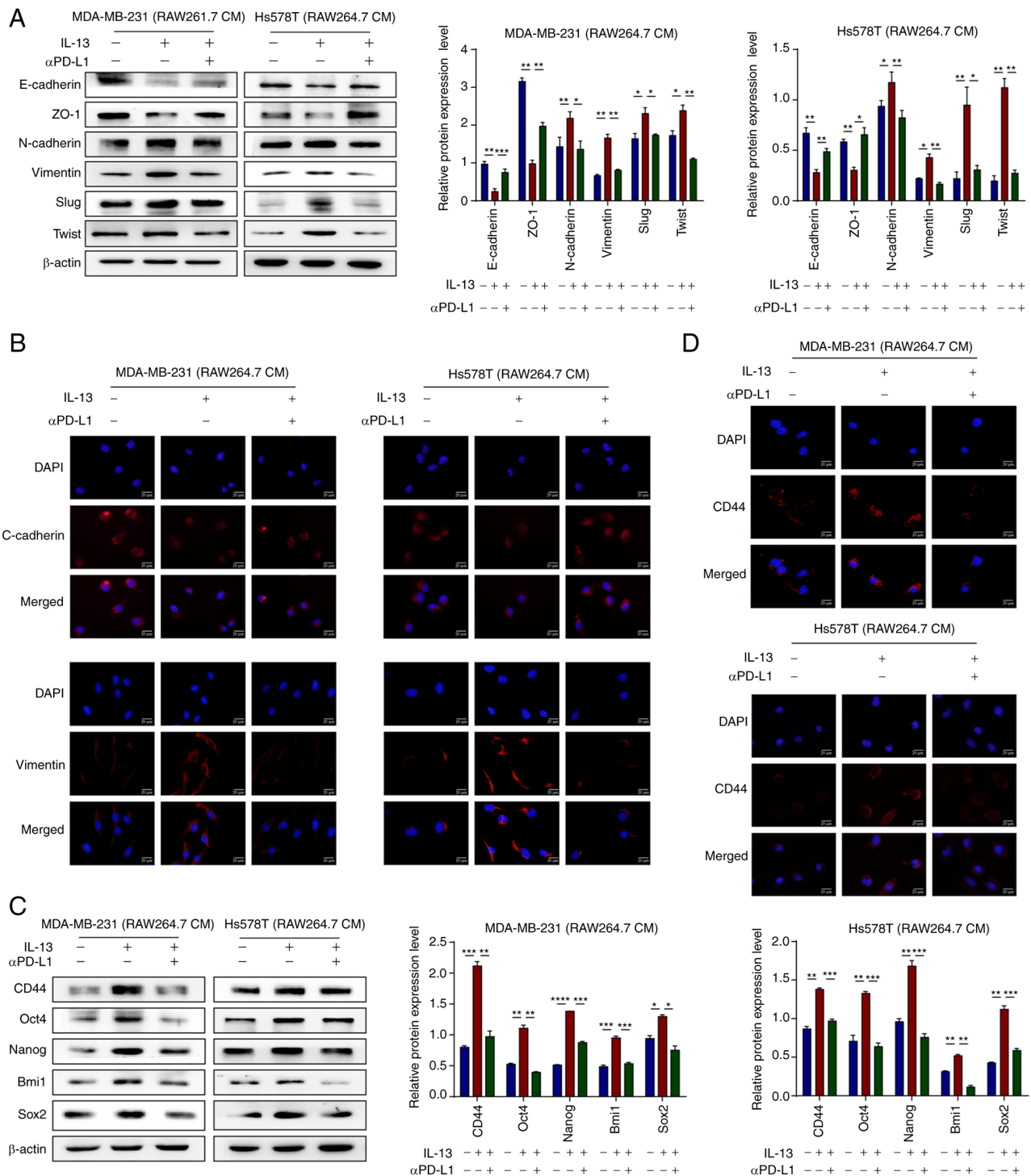
Figure 3. αPD-L1 inhibits the EMT process and the stemness of TNBC promoted by TAM/M2. (A) Protein expression levels of EMT markers, E-Cadherin, ZO-1, N-Cadherin, Vimentin, Slug and Twist, in MDA-MB-231 and Hs578T cells treated with CM, as determined using western blot analysis. (B) E-cadherin and vimentin protein expression levels in MDA-MB-231 and Hs578T cells treated with CM were analyzed using IF staining. The markers were all expressed in the cytoplasm (magnification, x400). (C) Protein expression levels of the stemness markers, CD44, Oct4, Nanog, Bmi1 and Sox2, in MDA-MB-231 and Hs578T cells treated with CM, as determined using western blot analysis. (D) CD44 protein expression levels in MDA-MB-231 and Hs578T cells treated with CM were assessed using IF staining. The markers were all expressed in the cytoplasm (magnification, x400). *P<0.05, **P<0.01, ***P<0.001 and ****P<0.0001. αPD-L1, programmed death-ligand 1 inhibitor; EMT, epithelial-mesenchymal transition; TAM/M2, tumor-associated macrophages/M2-type; ZO-1, zonula occludens-1; CM, conditional media; IF, immunofluorescence.

TNBC cells induce TAM/M2 polarization, and positive feedback promotes the malignant evolution of TNBC cells. To investigate whether TAM/M2 cells promote the malignant progression of TNBC cells in a co-culture system, a co-culture system was established and wound healing and

Transwell assays were performed. The results demonstrated that TAM/M2 promoted the migration of TNBC cells, whereas αPD-L1 reversed this phenomenon (Fig. 5A and B). To further investigate whether TAM/M2 directly induces the angiogenesis of TNBC, western blot analysis was performed.
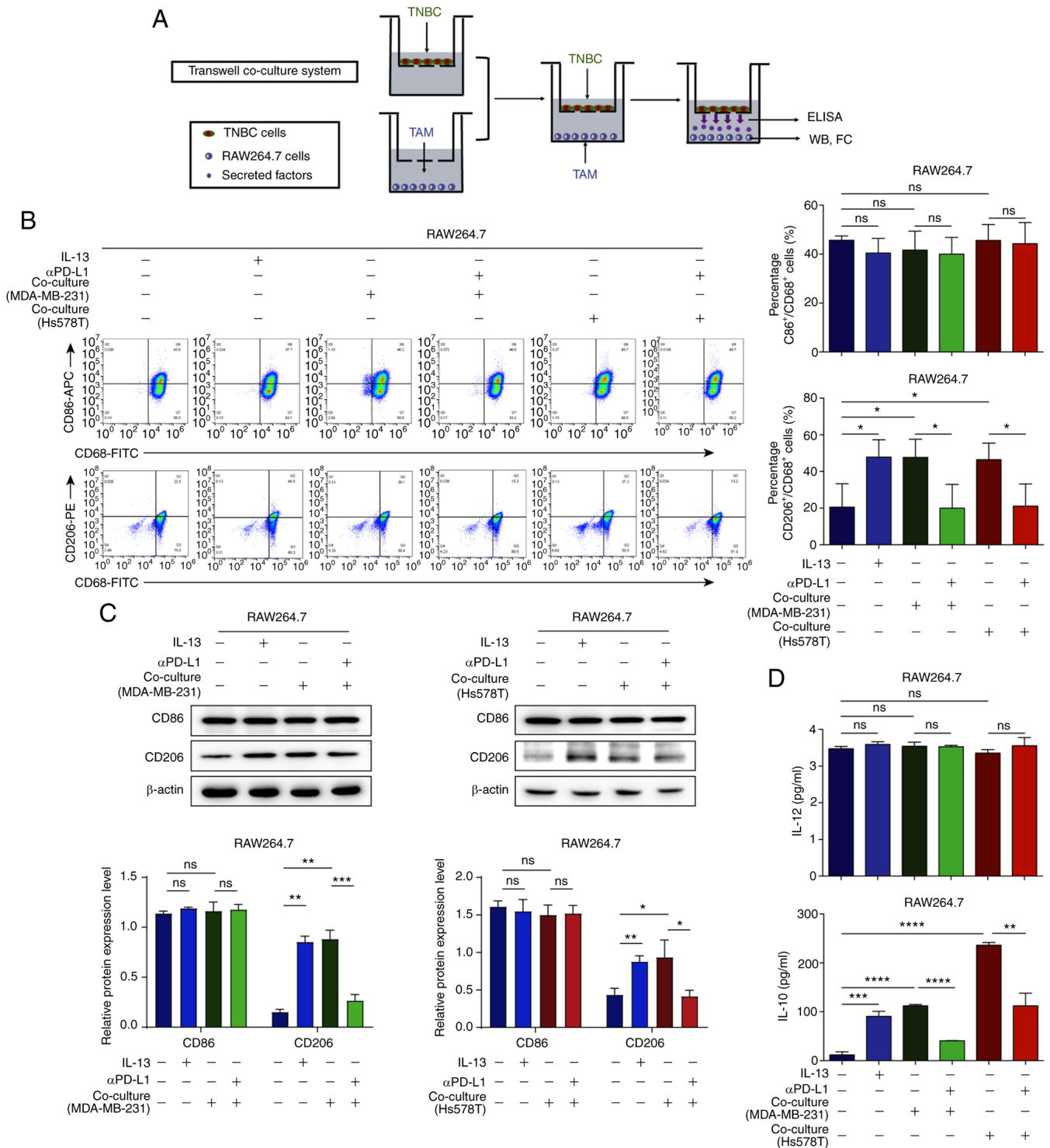
Figure 4. αPD-L1 reverses TAM/M2 polarization in the co-culture of TNBC cells and TAMs. (A) Schematic diagram of TNBC cells and the TAMs co-culture system. (B) RAW264.7 cells were co-cultured with MDA-MB-231 and Hs578T cells. The percentages of CD86⁺/CD68⁺ and CD206⁺/CD68⁺ treated with or without αPD-L1 in the co-culture system were determined using flow cytometry assay. (C) CD86 and CD206 protein expression levels, when the cells were treated with or without αPD-L1 in co-culture, were determined using western blot analysis. (D) IL-12 and IL-10 levels, in cells treated with or without αPD-L1 in co-culture, were assessed using ELISA. $^*P<0.05$, $^{**}P<0.01$, $^{***}P<0.001$, and $^{****}P<0.0001$. ns, not significant; αPD-L1, programmed death-ligand 1 inhibitor; TAM/M2, tumor-associated macrophages/M2-type; TNBC, triple-negative breast cancer.

The results demonstrated that TAM/M2 upregulated the protein expression levels of VEGF, MMP2 and MMP9 in the TNBC cells, whereas αPD-L1 reversed these effects (Fig. 5C). Furthermore, TAM/M2 upregulated the protein expression levels of mesenchymal and stemness markers in TNBC cells and downregulated those of epithelial markers, whereas αPD-L1 reversed the EMT process and the stemness of TNBC cells (Fig. 5D and E). On the whole, these data suggested that αPD-L1 potentially inhibited the migration and angiogenesis of TNBC cells via the regulation of the TAM polarization-mediated EMT process and cancer stemness.
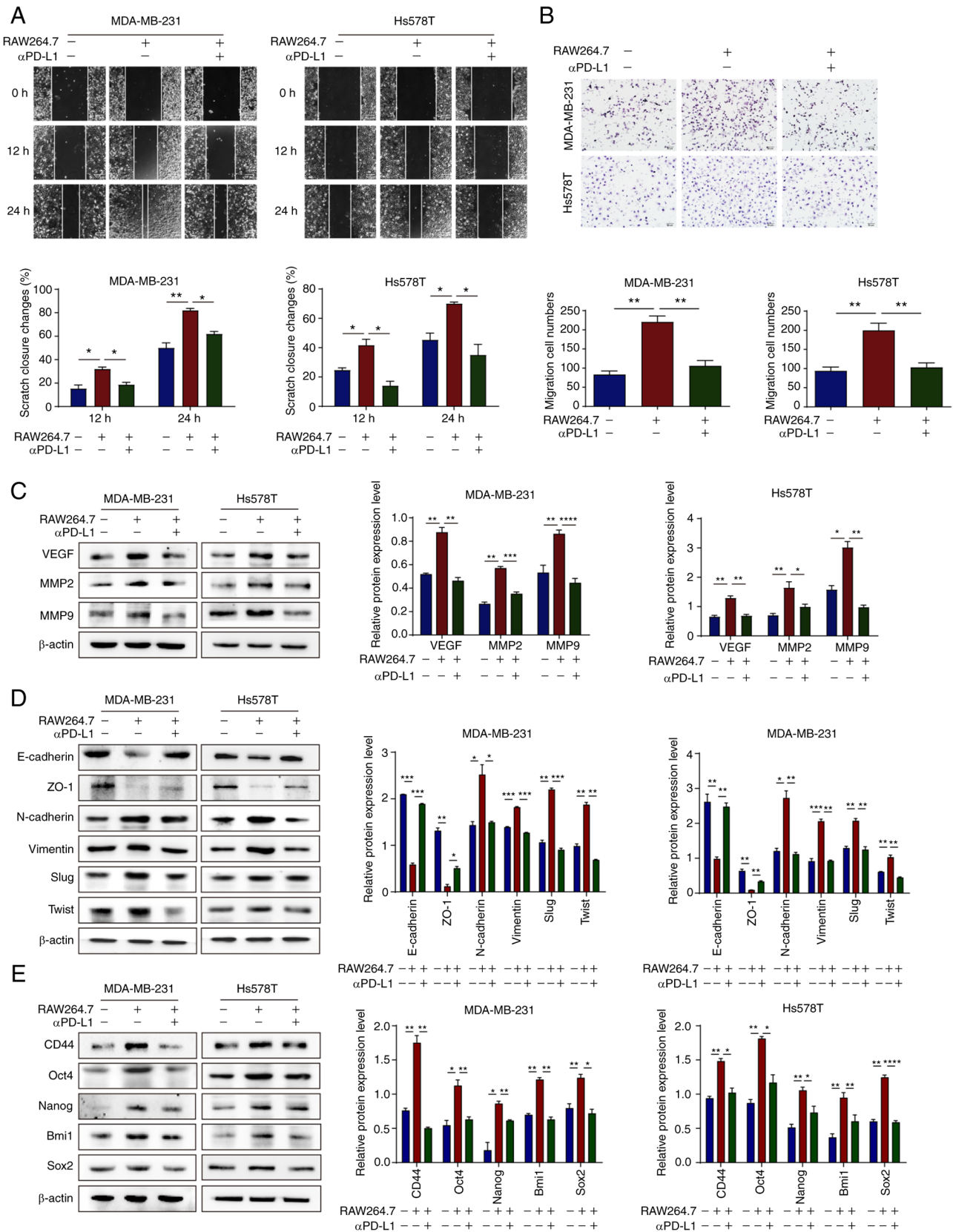
Figure 5. αPD-L1 reverses TNBC malignant evolution in the co-culture of TNBC cells and TAMs. (A and B) MDA-MB-231 and Hs578T cell migration capacity was assessed using wound healing and Transwell assays when the cells were treated with or without αPD-L1 in a co-culture system (magnification, x200). (C) Protein expression levels of VEGF, MMP2 and MMP9 in MDA-MB-231 and Hs578T cells, with or without αPD-L1 in a co-culture system, were determined using western blot analysis. (D) Protein expression levels of the EMT markers, E-cadherin, ZO-1, N-cadherin, vimentin, Slug and Twist, in MDA-MB-231 and Hs578T cells, with or without αPD-L1 in a co-culture system, were determined using western blot analysis. (E) Protein expression levels of the stemness markers, CD44, Oct4, Nanog, Bmi1 and Sox2 in MDA-MB-231 and Hs578T cells, with or without αPD-L1 in a co-culture system were determined using western blot analysis. $^*P<0.05$, $^{**}P<0.01$, $^{***}P<0.001$ and $^{****}P<0.0001$. αPD-L1, programmed death-ligand 1 inhibitor; TNBC, triple-negative breast cancer; TAM/M2, tumor-associated macrophages/M2-type; VEGF, vascular endothelial growth factor; EMT, epithelial-mesenchymal transition; ZO-1, zonula occludens-1.

aPD-L1 regulates TAM/M2 polarization by downregulating STAT3 phosphorylation and preventing its entry into the nucleus. To further investigate the molecular mechanisms through which αPD-L1 regulates TAM polarization, several immune-related signaling pathways were examined. The CEBPb, MAPK and STAT signaling pathways are all involved in TAM/M2 polarization (31,32). In the present study, western blot analysis was performed and the results demonstrated that IL-13, with or without αPD-L1, did not affect the protein expression levels of CEBPβ. However, IL-13 upregulated the protein expression levels of p-ERK, p-STAT6 and p-STAT3. Of note, the protein expression levels of p-ERK and p-STAT6 exhibited no notable changes following αPD-L1 treatment. However, the expression levels of p-STAT3 were significantly downregulated following αPD-L1 treatment (Figs. 6A and S1B). IL-13 binding with its receptor promotes STAT3 phosphorylation to form a dimer in the nucleus (33). The location of STAT3 and p-STAT3 was subsequently determined using IF staining and nucleoplasm separation assays. The results confirmed that IL-13 led to the translocation of STAT3 from the cytoplasm to the nucleus, whereas αPD-L1 led to the translocation of STAT3 from the nucleus to the cytoplasm (Fig. 6B-D).

aPD-L1 prevents lung metastasis in vivo by targeting TAM/M2. The effects of αPD-L1 on lung metastasis in subcutaneous and intravenous models of TNBC were then investigated. αPD-L1 was dissolved in PBS and administered to mice intraperitoneally at a dose of 200 μg and the control group was treated with PBS (Fig. 7A). There were no significant differences in tumor growth and body weight between the two groups in the TNBC subcutaneous models (Fig. 7B and C and F). However, αPD-L1 reduced the number of metastatic nodes on the lung tissue surface. H&E staining of the lung tissues further confirmed the presence of lung metastases (Fig. 7D and E). Similar results were obtained in the TNBC intravenous model (Fig. 7G-I). These data suggested that αPD-L1 potentially prevented lung metastasis in both subcutaneous and intravenous models of TNBC.

Subsequently, IHC and IF staining demonstrated that αPD-L1 reduced CD206 expression in the lung and tumor tissues, which suggested that αPD-L1 potentially inhibited TAM/M2 polarization *in vivo* (Fig. 7J and K). IHC staining further demonstrated that αPD-L1 upregulated the protein expression levels of E-cadherin, and downregulated the protein expression levels of vimentin, VEGF and CD44 (Fig. 7L-O). These data thus suggested that αPD-L1 potentially played a significant role in the evolution of TNBC (Fig. 8).

Discussion

The TME is complex and changeable and is closely associated with the occurrence and metastasis of tumors. TAMs are a key component of the TME (34). Cytokines, such as IL-10 and TGF-β are secreted by TAM/M2 and can inhibit the tumor immune response and promote tumor development (35). Tumor cells can also release biomolecules into the TME and promote TAM/M2 polarization. The number of TAM/M2 cells in tumor tissues is related to the malignant biological behavior and poor prognosis of various solid tumors (36).

Furthermore, the activation of immune regulatory site PD-1/PD-L1 plays a critical role in the process of immune cell recognition. Blocking the expression of PD-L1 in host immune cells has more prominent tumor-suppressive effects than inhibiting the expression of PD-L1 in tumor cells (24). Targeting TAMs is an effective therapeutic approach with which to modulate the activity of anti-PD-L1 agents in cancer treatment (37). This indicates that PD-L1 may play a role by directly regulating macrophage activity. The results of the present study suggested that αPD-L1 potentially reversed the expression levels of PD-L1, the TAM/M2 marker, CD206, and the levels of IL-10.

The receptor for advanced glycation end-products regulates the TME by recruiting TAMs and therefore promotes the progression and metastasis of TNBC (38). However, the effects of blocking PD-1/PD-L1 on TAMs in the process of tumor metastasis remain to be further elucidated. In the present study, the effects of αPD-L1 on tumor cell migration via the regulation of TAM polarization *in vitro* were investigated. The results indicated that αPD-L1 potentially reversed the migration of TNBC cells mediated by TAM/M2 polarization.

EMT contributes towards enhancing the capability of cancer cells to migrate and invade, which is critical in tumor metastasis. Numerous solid tumors have a large number of macrophages in the TME, which can promote tumor metastasis (39). Cancer stemness originates from the fusion of TAM/M2 and breast cancer cells, and these hybrid cells overexpress mesenchymal and cancer stemness markers (40). Therefore, tumor cells are likely to become CSCs following the EMT of cancer cells (41). PD-1/PD-L1 induces immunosuppression and promotes the EMT of cancer cells (42). The effects of αPD-L1 on the EMT and the stemness of cancer cells were investigated in the present study via the regulation of TAM polarization *in vitro* and *in vivo*. The results demonstrated that αPD-L1 potentially reversed the EMT process and the stemness of TNBC cells that were induced via TAM/M2 polarization.

Neovascularization in tumor tissues is an important condition for the metastasis of malignant tumors, and this process is regulated by various chemokines in the TME (43). Macrophages promote the secretion of VEGF by tumor cells to induce angiogenesis in local tumor tissues, which provides nutrition for tumor growth and metastasis (44). 4-Hydroxphenyl retinamide inhibits the TAM/M2 phenotype, which thereby inhibits the promotion of angiogenesis (45). The expression of VEGF can promote the metastasis of cancer cells (46). Furthermore, MMPs affect the expression of tumor cell adhesion molecules and promote tumor cell translocation beyond the basement membrane (47). The results of the present study demonstrated that αPD-L1 downregulated VEGF, MMP2 and MMP9 protein expression levels via the inhibition of TAM/M2 polarization. From the results of the present study, it was suggested that αPD-L1 reversed the angiogenesis of TNBC induced by TAM/M2 polarization. It can therefore be hypothesized that αPD-L1 can potentially inhibit tumor metastasis and angiogenesis.

The conversion of the macrophage phenotype is dependent on the activation of the signaling pathway response. The transcription factor CEBPb regulates the expression of early growth response protein 2 and participates in the polarization
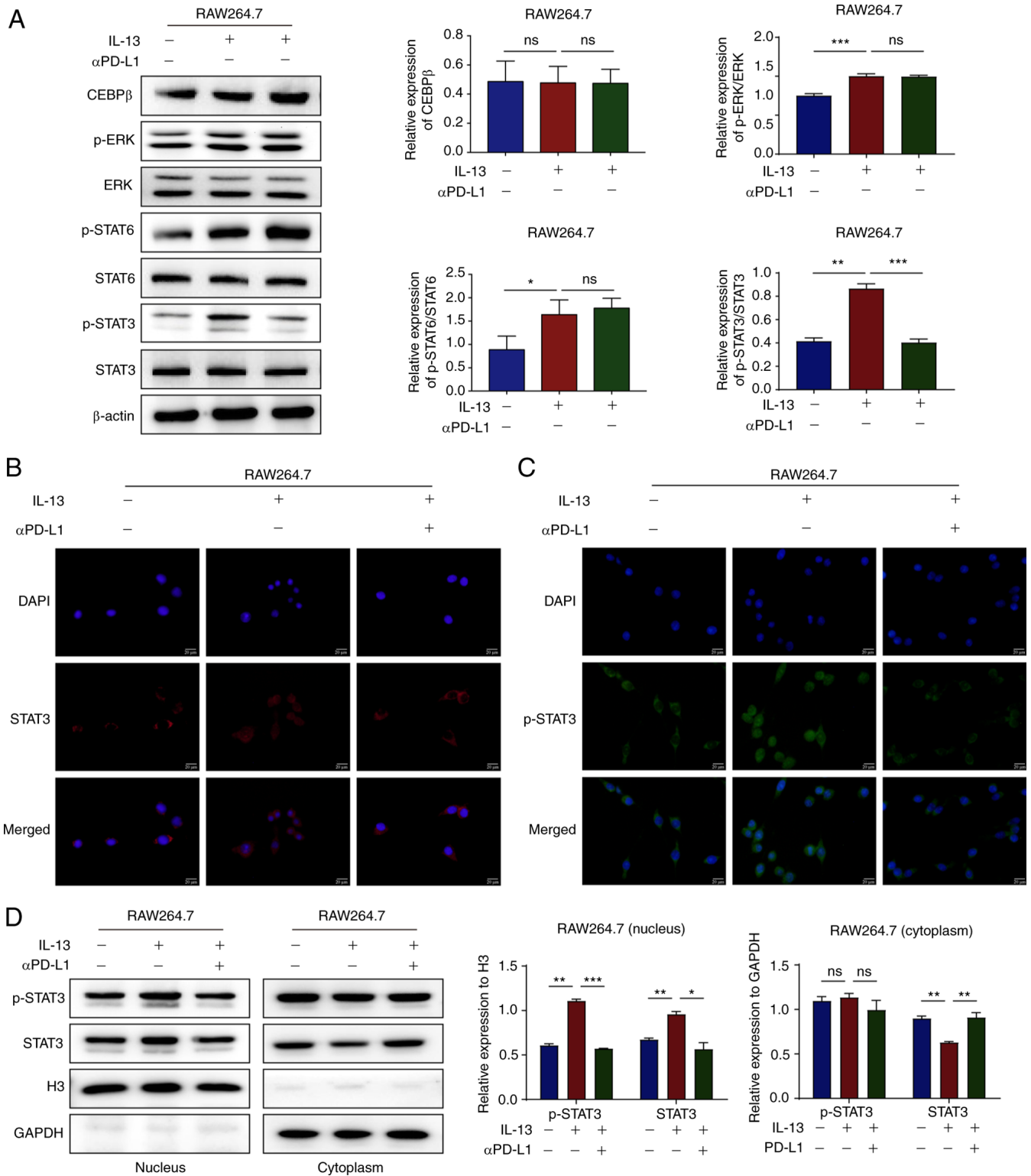
Figure 6. αPD-L1 inhibits TAM/M2 polarization via the prevention of STAT3 phosphorylation and nuclear translocation. (A) The protein expression levels of CEBPβ, p-ERK, ERK, p-STAT6, STAT6, p-STAT3 and STAT3 in RAW264.7 cells treated with IL-13 and/or αPD-L1 were determined using western blot analysis. (B and C) The protein expression levels and nuclear translocation of STAT3 and p-STAT3 in RAW264.7 cells treated with IL-13 and/or αPD-L1 were assessed using immunofluorescence staining (magnification, x400). (D) Cytosol and nuclear protein expression levels of STAT3 and p-STAT3 in RAW264.7 cells treated with IL-13 and/or αPD-L1 were assessed using western blot analysis. *P<0.05, **P<0.01 and ***P<0.001. ns, not significant; αPD-L1, programmed death-ligand 1 inhibitor; TAM/M2, tumor-associated macrophages/M2-type; CEBPβ, cAMP response element-binding protein/CCAAT-enhancer-binding protein β; p-, phosphorylated.

process of macrophages (48). A previous study demonstrated that tumor tissue promotes TAM/M2 polarization and induces the metastasis of lung cancer via the upregulation ERK

phosphorylation (36). Moreover, the STAT protein family regulates the biological behavior of tumor cells and immune cells via inflammatory mediators. These proteins play an
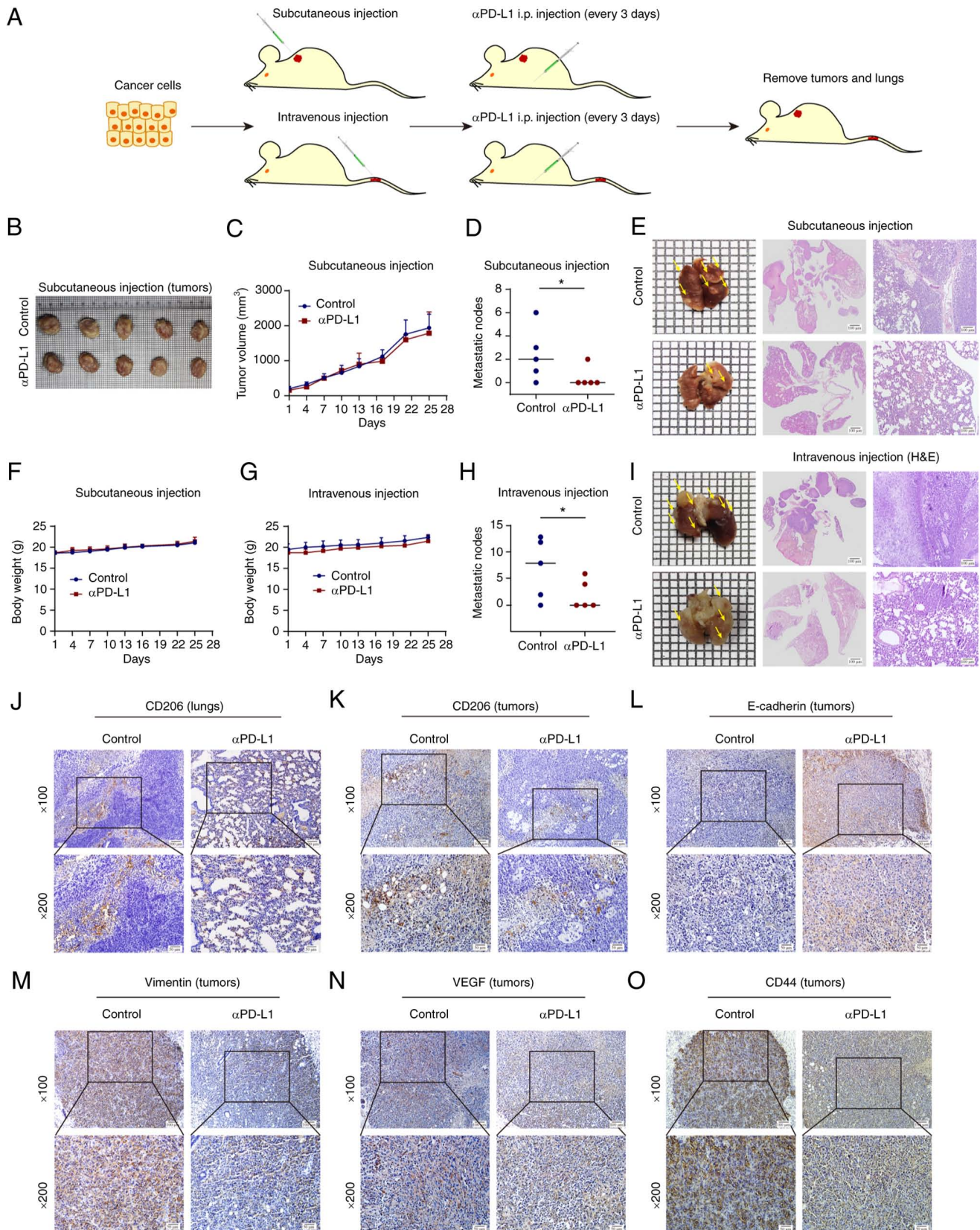
Figure 7. αPD-L1 inhibits lung metastasis *in vivo*. (A) Schematic diagram of the animal assays performed. (B and C) Tumor volume in the subcutaneous cell-transplanted mice was recorded over time throughout the animal assay. (D and H) The number of lung metastatic nodules was determined. (E) Lung metastases in mice that were subcutaneously injected with TNBC cells. Lung tissue images, H&E scan images and H&E magnification images (magnification, x100) are shown, respectively. (F and G) Body weight of subcutaneous and intravenous cell-transplanted mice was recorded over time throughout the animal assay. (I) Lung metastases in mice that were intravenously injected with TNBC cells. Lung tissue images, H&E scan images and H&E magnification images (magnification, x100) are shown, respectively. (J and K) CD206 protein expression levels in lung and tumor tissues were assessed using immunohistochemistry (magnification: upper panels, x100, lower panels, x200). (L-O) Protein expression levels of E-cadherin, vimentin, VEGF and CD44 in tumors tissues were determined using immunohistochemistry (magnification: upper panels, x100, lower panels, x200). *P<0.05. αPD-L1, programmed death-ligand 1 inhibitor; TNBC, triple-negative breast cancer; VEGF, vascular endothelial growth factor.
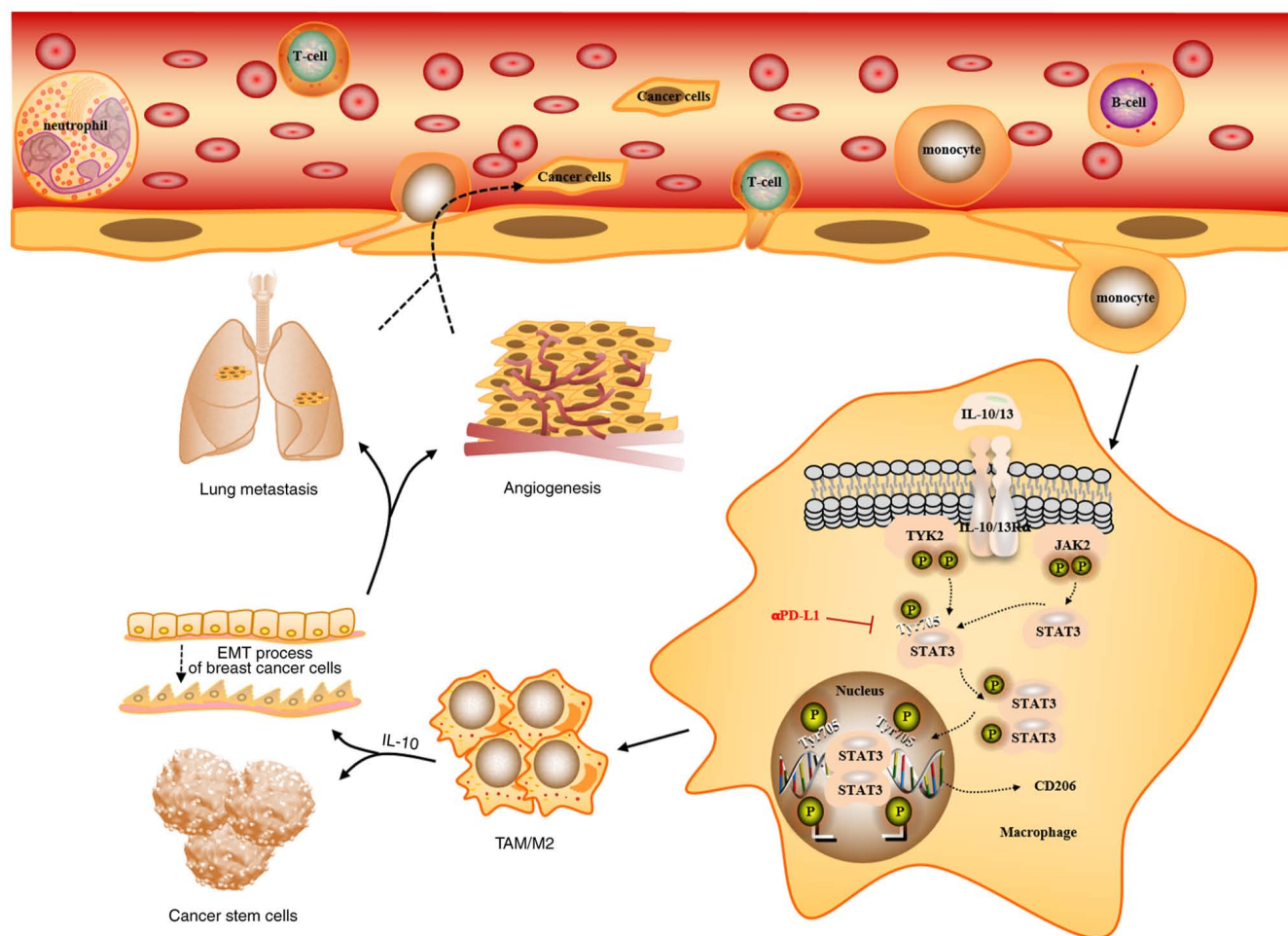
Figure 8. αPD-L1 potentially inhibits TAM/M2 polarization by blocking STAT3 entry into the nucleus, which potentially contributes to its anti-metastatic and anti-angiogenic function in triple-negative breast cancer. αPD-L1, programmed death-ligand 1 inhibitor; TAM/M2, tumor-associated macrophages/M2-type.

important role in the process of inflammation-cancer transformation. STAT3 signaling pathways serve an important role in TAM/M2 polarization (49,50). IL-13 binds to the IL-13 receptor on the surface of macrophages during TAM/M2 polarization and initiates the intracellular tyrosine kinase phosphorylation cascade. STAT3 is activated in the cytoplasm following phosphorylation at Y705 and S727. Activated STAT3 can therefore be transferred to the nucleus and promotes TAM/M2 polarization. The results of the present study indicated that the phosphorylation and nuclear translocation of STAT3 are potentially involved in the regulation of TAM/M2 polarization via αPD-L1.

In conclusion, the results of the present study demonstrated that αPD-L1 potentially inhibited TAM/M2 polarization *in vitro* and *in vivo*, which potentially contributed to its anti-metastatic and anti-angiogenic function in TNBC. Furthermore, STAT3 plays a crucial role in the effects of αPD-L1 on TAM/M2 polarization. Therefore, PD-L1 may be a promising biomarker for determining the prognosis of patients with TNBC and may provide a potential therapeutic target for TAMs in anti-metastatic treatment.

Acknowledgements

Not applicable.

Availability of data and materials

The datasets used and/or analyzed during the current study are available from the corresponding author on reasonable request.

Authors' contributions

TJ and MZ designed the experiments. ZM, RZ and XW performed the statistical analyses. ZM, RZ and XW performed the experiments. ZM and RZ wrote the manuscript. TF and MZ confirm the authenticity of all the raw data. All authors have read and approved the final manuscript.

Ethics approval and consent to participate

The present study was approved by the Animal Ethics Committee of Yanbian University (approval no. YD20220916004), and was performed according to the guidelines of the Committee on Animal Research and Ethics.

Patient consent for publication

Not applicable.

Competing interests

The authors declare that they have no competing interests.

References

1. Zuo TT, Zheng RS, Zeng HM, Zhang SW and Chen WQ: Female breast cancer incidence and mortality in China, 2013. Thorac Cancer 8: 214-218, 2017.
2. Sung H, Ferlay J, Siegel RL, Laversanne M, Soerjomataram I, Jemal A and Bray F: Global Cancer Statistics 2020: GLOBOCAN estimates of incidence and mortality worldwide for 36 cancers in 185 countries. CA Cancer J Clin 71: 209-249, 2021.
3. Shaikh S and Rasheed A: Predicting molecular subtypes of breast cancer with mammography and ultrasound findings: Introduction of Sono-mammometry score. Radiol Res Pract 2021: 6691958, 2021.
4. Jiagge EM, Ulintz PJ, Wong S, McDermott SP, Fossi SI, Suhan TK, Hoenerhoff MJ, Bensenhaver JM, Salem B, Dziubinski M, et al: Multiethnic PDX models predict a possible immune signature associated with TNBC of African ancestry. Breast Cancer Res Treat 186: 391-401, 2021.
5. Manjunath M and Choudhary B: Triple-negative breast cancer: A run-through of features, classification and current therapies. Oncol Lett 22: 512, 2021.
6. Li H, Fan X and Houghton J: Tumor microenvironment: The role of the tumor stroma in cancer. J Cell Biochem 101: 805-815, 2007.
7. Martinez-Reyes I and Chandel NS: Cancer metabolism: Looking forward. Nat Rev Cancer 21: 669-680, 2021.
8. Emami F, Pathak S, Nguyen TT, Shrestha P, Maharjan S, Kim JO, Jeong JH and Yook S: Photoimmunotherapy with cetuximab-conjugated gold nanorods reduces drug resistance in triple negative breast cancer spheroids with enhanced infiltration of tumor-associated macrophages. J Control Release 329: 645-664, 2021.
9. Mantovani A, Marchesi F, Malesci A, Laghi L and Allavena P: Tumour-associated macrophages as treatment targets in oncology. Nat Rev Clin Oncol 14: 399-416, 2017.
10. Adorno-Cruz V, Hoffmann AD, Liu X, Dashzeveg NK, Taftaf R, Wray B, Keri RA and Liu H: ITGA2 promotes expression of ACLY and CCND1 in enhancing breast cancer stemness and metastasis. Genes Dis 8: 493-508, 2021.
11. Turajlic S and Swanton C: Metastasis as an evolutionary process. Science 352: 169-175, 2016.
12. Deng Y, Hu JC, He SH, Lou B, Ding TB, Yang JT, Mo MG, Ye DY, Zhou L, Jiang XC, et al: Sphingomyelin synthase 2 facilitates M2-like macrophage polarization and tumor progression in a mouse model of triple-negative breast cancer. Acta Pharmacol Sin 42: 149-159, 2021.
13. Zhang XL, Hu LP, Yang Q, Qin WT, Wang X, Xu CJ, Tian GA, Yang XM, Yao LL, Zhu L, et al: CTHRC1 promotes liver metastasis by reshaping infiltrated macrophages through physical interactions with TGF-β receptors in colorectal cancer. Oncogene 40: 3959-3973, 2021.
14. Tang C, Lei X, Xiong L, Hu Z and Tang B: HMGA1B/2 transcriptionally activated-POU1F1 facilitates gastric carcinoma metastasis via CXCL12/CXCR4 axis-mediated macrophage polarization. Cell Death Dis 12: 422, 2021.
15. Pastushenko I and Blanpain C: EMT transition states during tumor progression and metastasis. Trends Cell Biol 29: 212-226, 2019.
16. Yang C, Dou R, Wei C, Liu K, Shi D, Zhang C, Liu Q, Wang S and Xiong B: Tumor-derived exosomal microRNA-106b-5p activates EMT-cancer cell and M2-subtype TAM interaction to facilitate CRC metastasis. Mol Ther 29: 2088-2107, 2021.
17. Clevers H: The cancer stem cell: Premises, promises and challenges. Nat Med 17: 313-319, 2011.
18. Chen Y, Tan W and Wang C: Tumor-associated macrophage-derived cytokines enhance cancer stem-like characteristics through epithelial-mesenchymal transition. Onco Targets Ther 11: 3817-3826, 2018.
19. Larionova I, Kazakova E, Gerashchenko T and Kzhyshkowska J: New angiogenic regulators produced by TAMs: Perspective for targeting tumor angiogenesis. Cancers (Basel) 13: 3253, 2021.
20. Long Y, Yu X, Chen R, Tong Y and Gong L: Noncanonical PD-1/PD-L1 axis in relation to the efficacy of Anti-PD therapy. Front Immunol 13: 910704, 2022.
21. Gatalica Z, Snyder C, Maney T, Ghazalpour A, Holterman DA, Xiao N, Overberg P, Rose I, Basu GD, Vranic S, et al: Programmed cell death 1 (PD-1) and its ligand (PD-L1) in common cancers and their correlation with molecular cancer type. Cancer Epidemiol Biomarkers Prev 23: 2965-2970, 2014.
22. Cimino-Mathews A, Foote JB and Emens LA: Immune targeting in breast cancer. Oncology (Williston Park) 29: 375-385, 2015.
23. Moser JC and Hu-Lieskovan S: Mechanisms of resistance to PD-1 checkpoint blockade. Drugs 80: 459-465, 2020.
24. Noguchi T, Ward JP, Gubin MM, Arthur CD, Lee SH, Hundal J, Selby MJ, Graziano RF, Mardis ER, Korman AJ and Schreiber RD: Temporally Distinct PD-L1 expression by tumor and host cells contributes to immune escape. Cancer Immunol Res 5: 106-117, 2017.
25. Juneja VR, McGuire KA, Manguso RT, LaFleur MW, Collins N, Haining WN, Freeman GJ and Sharpe AH: PD-L1 on tumor cells is sufficient for immune evasion in immunogenic tumors and inhibits CD8 T cell cytotoxicity. J Exp Med 214: 895-904, 2017.
26. Deng L, Liang H, Burnette B, Beckett M, Darga T, Weichselbaum RR and Fu YX: Irradiation and anti-PD-L1 treatment synergistically promote antitumor immunity in mice. J Clin Invest 124: 687-695, 2014.
27. Fu LQ, Du WL, Cai MH, Yao JY, Zhao YY and Mou XZ: The roles of tumor-associated macrophages in tumor angiogenesis and metastasis. Cell Immunol 353: 104119, 2020.
28. Wang W, Zhao Y, Yao S, Cui X, Pan W, Huang W, Gao J, Dong T and Zhang S: Nigericin inhibits epithelial ovarian cancer metastasis by suppressing the cell cycle and Epithelial-mesenchymal transition. Biochemistry (Mosc) 82: 933-941, 2017.
29. Stankevicius V, Kunigenas L, Stankunas E, Kuodyte K, Strainiene E, Cicenas J, Samalavicius NE and Suziedelis K: The expression of cancer stem cell markers in human colorectal carcinoma cells in a microenvironment dependent manner. Biochem Biophys Res Commun 484: 726-733, 2017.
30. Wylie PG and Bowen WP: Determination of cell colony formation in a high-content screening assay. Clin Lab Med 27: 193-199, 2007.
31. Lawrence T and Natoli G: Transcriptional regulation of macrophage polarization: Enabling diversity with identity. Nat Rev Immunol 11: 750-761, 2011.
32. Neamatallah T: Mitogen-activated protein kinase pathway: A critical regulator in Tumor-associated macrophage polarization. J Microsc Ultrastruct 7: 53-56, 2019.
33. LaPorte SL, Juo ZS, Vaclavikova J, Colf LA, Qi X, Heller NM, Keegan AD and Garcia KC: Molecular and structural basis of cytokine receptor pleiotropy in the interleukin-4/13 system. Cell 132: 259-272, 2008.
34. Boutilier AJ and Elsawa SF: Macrophage polarization states in the tumor microenvironment. Int J Mol Sci 22: 6995, 2021.
35. Ma YY, He XJ, Wang HJ, Xia YJ, Wang SL, Ye ZY and Tao HQ: Interaction of coagulation factors and tumor-associated macrophages mediates migration and invasion of gastric cancer. Cancer Sci 102: 336-342, 2011.
36. Sami E, Paul BT, Koziol JA and ElShamy WM: The immunosuppressive microenvironment in BRCA1-IRIS-overexpressing TNBC tumors is induced by bidirectional interaction with tumor-associated macrophages. Cancer Res 80: 1102-1117, 2020.
37. Santoni M, Romagnoli E, Saladino T, Foghini L, Guarino S, Capponi M, Giannini M, Cognigni PD, Ferrara G and Battelli N: Triple negative breast cancer: Key role of Tumor-associated macrophages in regulating the activity of anti-PD-1/PD-L1 agents. Biochim Biophys Acta Rev Cancer 1869: 78-84, 2018.
38. Nasser MW, Wani NA, Ahirwar DK, Powell CA, Ravi J, Elbaz M, Zhao H, Padilla L, Zhang X, Shilo K, et al: RAGE mediates S100A7-induced breast cancer growth and metastasis by modulating the tumor microenvironment. Cancer Res 75: 974-985, 2015.
39. Nieto MA, Huang RY, Jackson RA and Thiery JP: EMT: 2016. Cell 166: 21-45, 2016.
40. Li B, Lu Y, Yu L, Han X, Wang H, Mao J, Shen J, Wang B, Tang J, Li C and Song B: miR-221/222 Promote cancer stem-like cell properties and tumor growth of breast cancer via targeting PTEN and sustained Akt/NF-κB/COX-2 activation. Chem Biol Interact 277: 33-42, 2017.

41. Zhou Y, Chen D, Qi Y, Liu R, Li S, Zou H, Lan J, Ju X, Jiang J, Liang W, *et al*: Evaluation of expression of cancer stem cell markers and fusion gene in synovial sarcoma: Insights into histogenesis and pathogenesis. Oncol Rep 37: 3351-3360, 2017.

42. Wu T, Tang C, Tao R, Yong X, Jiang Q and Feng C: PD-L1-mediated immunosuppression in oral squamous cell carcinoma: Relationship with macrophage infiltration and epithelial to mesenchymal transition markers. Front Immunol 12: 693881, 2021.

43. Samples J, Willis M and Klauber-Demore N: Targeting angiogenesis and the tumor microenvironment. Surg Oncol Clin N Am 22: 629-639, 2013.

44. Barnett FH, Rosenfeld M, Wood M, Kiosses WB, Usui Y, Marchetti V, Aguilar E and Friedlander M: Macrophages form functional vascular mimicry channels in vivo. Sci Rep 6: 36659, 2016.

45. Dong R, Gong Y, Meng W, Yuan M, Zhu H, Ying M, He Q, Cao J and Yang B: The involvement of M2 macrophage polarization inhibition in fenretinide-mediated chemopreventive effects on colon cancer. Cancer Lett 388: 43-53, 2017.

46. Wang H, Yung MMH, Ngan HYS, Chan KKL and Chan DW: The impact of the tumor microenvironment on macrophage polarization in cancer metastatic progression. Int J Mol Sci 22: 6560, 2021.

47. Watroba S, Wisniowski T, Bryda J and Kurzepa J: The role of matrix metalloproteinases in pathogenesis of human bladder cancer. Acta Biochim Pol 68: 547-555, 2021.

48. Veremeyko T, Yung AWY, Anthony DC, Strekalova T and Ponomarev ED: Early growth response Gene-2 is essential for M1 and M2 macrophage activation and plasticity by modulation of the transcription factor CEBPβ. Front Immunol 9: 2515, 2018.

49. Xu J, Zhang J, Zhang Z, Gao Z, Qi Y, Qiu W, Pan Z, Guo Q, Li B, Zhao S, *et al*: Hypoxic glioma-derived exosomes promote M2-like macrophage polarization by enhancing autophagy induction. Cell Death Dis 12: 373, 2021.

50. Qian M, Wang S, Guo X, Wang J, Zhang Z, Qiu W, Gao X, Chen Z, Xu J, Zhao R, *et al*: Hypoxic glioma-derived exosomes deliver microRNA-1246 to induce M2 macrophage polarization by targeting TERF2IP via the STAT3 and NF-κB pathways. Oncogene 39: 428-442, 2020.